Research Article Vol. 5, No. 9 / 15 Sep 2026 / Optics Continuum 3054
OPTICS CONTINUUM

Laser frequency stabilization to water vapor for trapped ion quantum technology

STEVEN OLMSCHENK*

Department of Physics and Astronomy, Denison University, 100 West College Street, Granville, OH 43023, USA
*steven.olmschenk@denison.edu

Abstract: We stabilize the frequency of a diode laser operating near 1389.8 nm to an absorption line in water vapor. We measure the Allan deviation of the system to be 1.8×10^{-10} at a 20-minute averaging time. The beatnote between two nearly identical systems deviates by $<\pm 1.6$ MHz over 15.5 hours. The all-fiber optical setup may facilitate compact and alignment-free laser systems for field-deployable trapped ion quantum technology.

1. Introduction

Stabilizing the frequency of a laser to an external reference is an essential prerequisite for many applications in quantum information [1], laser cooling [2–4], quantum metrology [5,6], and quantum sensing [7,8]. One of the most advanced platforms for these applications in quantum technology are trapped atomic ions, due to the long coherence times and precise control achieved in these systems [9,10]. Trapped ion systems use a variety of external references for laser frequency stabilization, including hollow cathode lamps [11,12], optical cavities [13–16], wavelength meters [17–19], and molecular gas cells [20–23]. A range of techniques can be also used to provide feedback to the laser, such as side-of-fringe, wavelength modulation spectroscopy, frequency modulation spectroscopy, saturated absorption spectroscopy, and modulation transfer spectroscopy [24,25]. However, as quantum technologies move from the lab into the field, there is a growing need for laser frequency stabilization amenable to compact system design and maintenance-free operation [26,27].

Gas cells of water vapor are an excellent option for an external frequency reference in the near-infrared due to the large number of absorption lines in the range of 0.7-1.5 μm [28,29]. Prior work using water vapor includes stabilizing the frequency of a laser near 791 nm using wavelength modulation spectroscopy [30], near 820 nm using wavelength modulation spectroscopy [31–33], near 935 nm using frequency modulation spectroscopy [34] and wavelength modulation spectroscopy [35–37], near 1370 nm using wavelength modulation spectroscopy [38,39], near 1390 nm using software profile fitting [40], near 1460 nm using wavelength modulation spectroscopy [41], and near 1520 nm using wavelength modulation spectroscopy [42]. Doppler-free saturated absorption spectroscopy and related techniques have also been used for laser stabilization near 1390 nm by utilizing the power enhancement of an optical cavity to saturate the transition [43–47].

Here we use wavelength modulation spectroscopy with a sideband of an electro-optic modulator (EOM) to stabilize the frequency of a diode laser operating near 1389.8 nm (vacuum) to an absorption line in water vapor. We measure the beatnote between two nearly identical systems to characterize the frequency fluctuations and long-term stability of the laser. The all-fiber optical setup eliminates the need for spatial optical alignment, which should enable compact system designs and maintenance-free operation. The laser operates at one of the wavelengths for cooling doubly-ionized lanthanum, a recently proposed qubit candidate [48], though the technique is applicable to a range of laser frequencies integral to quantum technology based on trapped atomic ions.

#603828 https://doi.org/10.1364/OPTCON.603828
Journal © 2026 Received 27 Apr 2026; revised 31 Jul 2026; accepted 4 Aug 2026; published 8 Sep 2026

OPTICS CONTINUUM

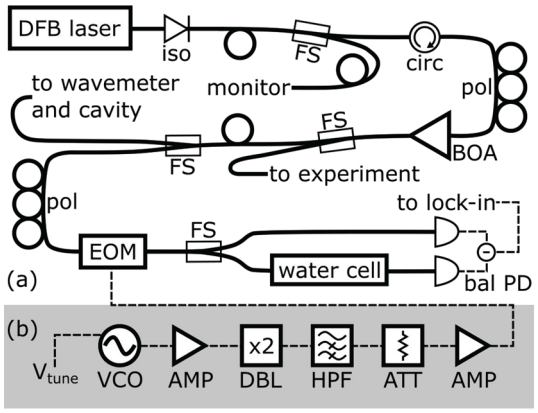

Fig. 1. The experimental setup for frequency-stabilizing the laser. (a) The optical setup. An isolated distributed feedback (DFB) diode laser produces light that is amplified by a booster optical amplifer (BOA). A fraction of this light is then passed to an electro-optic modulator (EOM) for wavelength modulation spectroscopy of water vapor in a fiber-coupled vapor cell (water cell). The signal is demodulated by a lock-in amplifier and sent to an analog proportional-integral-derivative (PID) controller, which provides feedback to stabilize the frequency of the laser. Optical fibers are drawn as solid, thick, curved lines; electrical connections are drawn as straight, thin, dashed lines. FS is fiber splitter; iso is isolator; circ is circulator; pol is polarization controller; bal PD is balanced photodiode. (b) The radiofrequency (rf) setup to drive the EOM. The signal from a voltage-controlled oscillator (VCO) is amplified, frequency-doubled, filtered, attenuated, amplified again, and then sent to the EOM to generate a first-order sideband at the frequency of the water absorption line. A tuning voltage (V_{tune}) is provided by a benchtop function generator (not shown) to set the frequency of the VCO, and is dithered at 11.4 kHz for wavelength modulation spectroscopy. AMP is amplifier; DBL is frequency doubler; HPF is high-pass filter; ATT is attenuator.

2. Experimental setup

The diode laser is stabilized to an absorption line in water vapor using an all-fiber optical setup, illustrated in Fig. 1(a). The diode laser under test is a fiber-coupled distributed feedback (DFB) laser (QPhotonics QDFBLD-1390-10) with an output power of about 8 mW at a 27 mA drive current at 23 °C. The laser linewidth is measured to be 6.9 ± 0.3 MHz using a delayed self-heterodyne technique with a 1 km delay line [49] (see also Appendix A). Following an in-line isolator, 90/10 splitter (for monitoring the laser directly), and circulator, the resulting 4.6 mW of light is amplified using a fiber-coupled booster optical amplifier (BOA, Thorlabs BOA1036P). The polarization of the light into the BOA is manually optimized using a fiber paddle polarization controller (Thorlabs FPC030). At a drive current of 250 mA the BOA outputs 50.1 mW, where 45.7 mW (91%) is sent to an ultra-high vacuum chamber for future experiments. The remaining power is split between a path leading to a wavemeter (Bristol 521-NIR) and lab-built Fabry-Pérot cavity for monitoring the laser (2.1 mW), and the water vapor frequency stabilization setup characterized here (2.3 mW). Another fiber paddle is used to manually control the polarization of the light used for frequency stabilization, and then the light is sent through a fiber-coupled EOM (Thorlabs LN65S-FC) to generate a sideband at the water vapor absorption line, with optical transmission of about 0.4 (about 0.9 mW transmitted). After the EOM, the light is split approximately equally between two paths: one path passes through a 10 Torr, fiber-coupled, multi-pass, water vapor cell with a path length of 48 cm (Wavelength References H2O-H(48)-10-FCAPC) and optical transmission of about 0.7 off-resonance (0.3 on-resonance); the other path goes directly to the detector. The light is measured by a lab-built

OPTICS CONTINUUM

balanced photodiode detector (based on the design in Ref. [50]), with about 0.3 mW reaching the detector from each path. All fiber components have FC/APC connectors, and are connected using standard simplex adapters (e.g. Precision Micro-Optics FFAD-31213) with typical optical transmission of about 0.9 at each connection.

The EOM is driven by the radiofrequency (rf) components illustrated in Fig. 1(b) to generate first-order sidebands at about ±10.5 GHz. A voltage-controlled oscillator (VCO, Mini-Circuits ZX95-5363C-S+) produces an rf signal of about -3 dBm at 5.23 GHz. The rf signal is amplified (Mini-Circuits ZX60-V62+) to about +8 dBm, frequency doubled (Mini-Circuits ZX90-2-24-S+), filtered (Mini-Circuits VHF-8400+) to remove frequencies <6.0 GHz, attenuated (Mini-Circuits VAT-6+) to about -20 dBm, amplified again (Mini-Circuits ZX60-183A-S+) to about +10 dBm, and then sent to the EOM, producing sidebands on the laser light with a modulation depth of about 0.3. The VCO frequency is swept over 0.15 GHz at a modulation frequency of 11.4 kHz for lock-in detection. The lock-in amplifier (EG&G 5210) is operated in high stability mode, with a sensitivity of 300 mV, 11.4 kHz bandpass filter, f and $2f$ line filters, and a time constant of 3 ms to produce the signal used for spectroscopy and frequency stabilization.

3. Data and analysis

We observe the water absorption line using wavelength modulation spectroscopy. The frequency of the laser is scanned by ramping the temperature, producing the dispersion-like lineshape shown in Fig. 2 as the EOM first-order sideband (about 10.5 GHz less than the laser frequency) is scanned across the water vapor resonance. The center of this dispersion-like lineshape, where the inverse of the slope is about 34 MHz/V, is used to stabilize the frequency of the DFB laser.

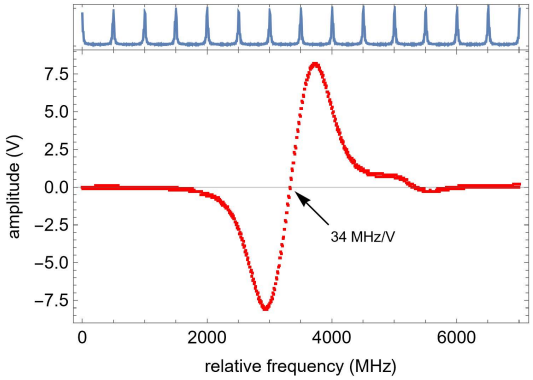

Fig. 2. The measured dispersion-like lineshape as the EOM first-order sideband is scanned across the water absorption line as the laser is temperature tuned. The small lineshape that appears around 5250 MHz is a result of the opposite EOM first-order sideband resonant with a separate, weak, water absorption line (see Appendix B). The small plot at the top shows transmission peaks through a Fabry-Pérot cavity with a free-spectral range of 500.7 MHz [51] and finesse of about 20, which is used to set the frequency scale.

The frequency stability is characterized by recording the beatnote between two laser systems. In this case, a second DFB laser near 1389.8 nm is frequency-stabilized using a separate optical and rf setup nearly identical to the first, though with an EOM sideband frequency of about 7.5 GHz, and serves as a reference frequency. The beatnote frequency between the two lasers systems is detected by a fast photodiode (Thorlabs DET08CFC) and measured by a spectrum analyzer (Spectran HF-60105 V4 X) with an average sweep time of about 3 s. The resulting spectra are fit to Lorentzian profiles to obtain the central beat frequency at each time stamp. The beatnote is recorded with the laser under test both free-running and frequency-stabilized (locked) for about

OPTICS CONTINUUM

15.5 hours, with the resulting frequency deviations shown in Fig. 3. In the locked case, the beatnote between the two stabilized laser systems deviates by $< \pm 1.6$ MHz (standard deviation 0.4 MHz) over the entire measurement interval. In the case the laser under test is free-running (no feedback from water vapor wavelength modulation spectroscopy), the frequency deviations are much larger, and the periodic cycling of the lab environmental control (temperature and humidity) is clearly evident.

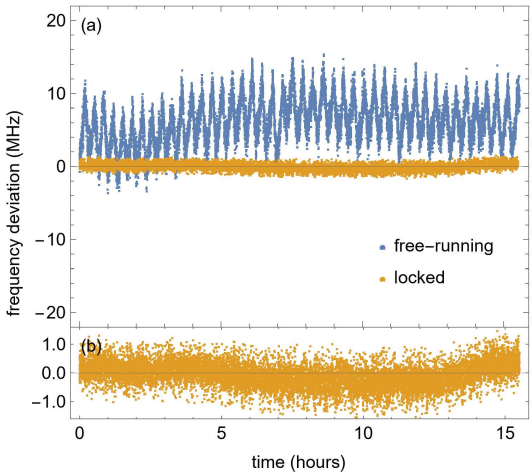

Fig. 3. The change in the beatnote frequency (frequency deviation) between the laser under test and the reference laser as a function of time, where the nominal beatnote frequency is 2941 MHz. (a) The beatnote frequency deviation is recorded both with the laser under test free-running and locked (frequency-stabilized) for about 15.5 hours. (The reference laser is locked for both cases.) (b) A zoomed-in plot of the change in the beatnote frequency with the laser under test locked, which shows that the beatnote deviates by $< \pm 1.6$ MHz (standard deviation 0.4 MHz) during the measurement interval.

The time variation of the beatnote frequency is used to calculate the overlapping Allan deviation [52] at multiple averaging times. Here we determine the Allan deviation for the frequency-stabilized laser under test by assuming two identical units (the laser under test and the reference laser), allowing the calculated Allan deviation of the beatnote signal to be divided by $\sqrt{2}$ to get the Allan deviation for the frequency-stabilized laser under test [52], with the results shown in Fig. 4. This Allan deviation is less than 8.1×10^{-10} at all averaging times, and reaches a minimum of 1.8×10^{-10} at a 20-minute averaging time. Beyond a 20-minute averaging time, the Allan deviation rises due to the remaining frequency drift of the system. When the laser under test is free-running, the Allan deviation is $>2.3 \times 10^{-9}$ at all averaging times.

OPTICS CONTINUUM

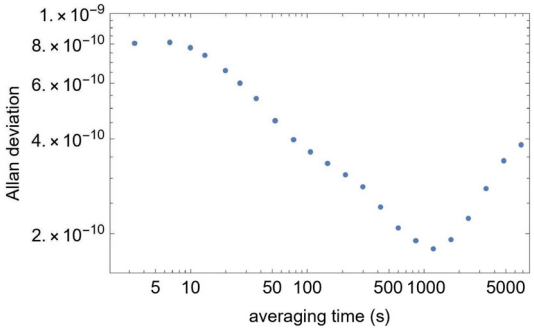

Fig. 4. The overlapping Allan deviation for the frequency-stabilized laser under test at several averaging times, calculated using the variation of the beatnote frequency between the laser under test and the reference laser. A minimum Allan deviation of 1.8×10^{-10} is reached at a 20-minute averaging time.

4. Discussion and conclusion

Laser frequency stability is an important metric for cooling trapped atomic ions. In most cases, trapped ion systems operate in a regime where the laser linewidth is less than the atomic linewidth of the cooling transition, thereby requiring that frequency excursions of the laser are less than the atomic linewidth to maintain the proper gradient for Doppler cooling. As most trapped ions are laser cooled using atomic transitions with linewidths on the order of $\sim$ 10 MHz (which also may be broadened due to incident power or external magnetic fields), this typically leads to the requirement that laser frequency deviations are less than a few MHz [11,12,18,19,21,23]. More generally, though, laser cooling only requires that the laser frequency is stabilized within either the linewidth of the atomic transition or the linewidth of the laser, with the caveat that if the laser linewidth is greater than the atomic linewidth the minimum temperature attainable by Doppler cooling will be limited by the laser linewidth [53]. The frequency stability required for driving transitions to depopulate metastable levels, returning the atom to the primary cooling transition (repump transitions), is typically less stringent [54].

While the frequency stability measured here is already better than the linewidth of the laser, and therefore applicable to laser cooling, future modifications could improve this system further. The majority of the observed frequency drift is most likely caused by residual amplitude modulation (RAM), a well-known issue with EOMs. Providing active feedback to the EOM can reduce RAM [55–57] and may improve the frequency stability of the system. Additionally, while simple passive thermal isolation of the VCO used to generate the EOM sideband limits deviations of the VCO central frequency to $< \pm 0.1$ MHz, exchanging the VCO for a digital frequency synthesizer may further reduce the impact of environmental changes on the sideband frequency. Also, using only polarization-maintaining fibers may eliminate the need for manual optimization of the polarization, and splicing together fiber components could reduce connection losses. Finally, although comparing two similar systems is a standard method for evaluating laser stability and the method employed here, the possibility of common-mode drifts would be mitigated by comparing to different types of stable references, such as a high finesse cavity, frequency comb, or disparate atomic or molecular lines.

The system demonstrated here may be useful for applications in quantum technology. The laser operates at 1389.8 nm, providing the first demonstration of a frequency-stabilized laser system applicable to cooling/repumping doubly-ionized lanthanum [48]. Moreover, the technique is applicable to a range of laser frequencies for trapped atomic ion quantum technology, as listed in Table 1. Besides its application in quantum technology, the system also may be useful

OPTICS CONTINUUM

for spectroscopic atmospheric measurements related to weather and climate using differential absorption lidar (DIAL), where stabilized laser frequencies allow for simultaneous absorption measurements on- and off-resonance of a water absorption line [64]. Altogether, this fiber-based optical setup facilitates compact designs and maintenance-free operation, advancing the goal of robust, field-deployable technologies.

Table 1. Selected trapped ion laser wavelengths near water vapor absorption lines

	λ_{ion} (nm)	E_{ion}[a] (cm^{-1})	E_{abs} (cm^{-1})	S_{abs}[b] (cm/molecule)	$\lvert\Delta f\rvert$[c] (GHz)
Be^+	939.40[d]	10645.11[d]	10644.71	2.5×10^{-23}	11.9
La^{2+}	1389.83	7195.14	7194.81	3.2×10^{-21}	10.0
	1410.00	7092.18	7092.50	1.2×10^{-21}	9.4
Mg^+	1118.54[e]	8940.22[e]	8941.51	5.6×10^{-22}	38.8
Tm^+	944.04[f]	10592.72	10592.87	2.7×10^{-22}	4.4
	1152.55[f]	8676.39	8675.78	5.1×10^{-22}	18.3
Yb^+	935.19[g]	10693.06	10691.77	1.6×10^{-23}	38.8

[a]Laser wavelengths (λ_{ion}) and energies (E_{ion}) to address ion transitions are presented using the values in Ref. [58]; values for addressing a specific isotope or hyperfine manifold may vary.
[b]Water vapor absorption line energies (E_{abs}) and intensities (S_{abs}) are from Ref. [29].
[c]Only absorption lines within 40 GHz of an ion transition were considered.
[d]Fundamental wavelength and energy for a tripled laser system, such as Ref. [59].
[e]Fundamental wavelength and energy for a quadrupled laser system, such as Ref. [60,61].
[f]See Ref. [62] for the proposed laser cooling and repumping scheme.
[g]See also water vapor absorption lines for Yb^+ laser frequency stabilization proposed by Ref. [63].

Appendices

A. Laser linewidth

We measure the laser linewidth both free-running (unlocked) and frequency-stabilized (locked) using a delayed self-heterodyne technique [49]. Light from the laser is split approximately equally between a path with a 1 km fiber delay line and a path with a fiber EOM driven at 675 MHz. After the two paths are recombined, the output is detected by a fast photodiode (Thorlabs DET08CFC) and measured by a spectrum analyzer (Spectran HF-60105 V4 X) with an average sweep time of about 26 s. An example of the delayed self-heterodyne spectrum is shown in Fig. 5. Six spectra are collected for both the free-running (unlocked) and frequency-stabilized (locked) laser and fit to Lorentzian profiles, allowing the laser linewidth to be calculated as 6.6 ± 0.4 MHz (unlocked) and 7.1 ± 0.3 MHz (locked). The two values of the linewidth are consistent with each other, as expected given the limited bandwidth of the feedback, and therefore we note the average of these measurements, 6.9 ± 0.3 MHz, as the linewidth of the laser in Sec. 2 above.

OPTICS CONTINUUM

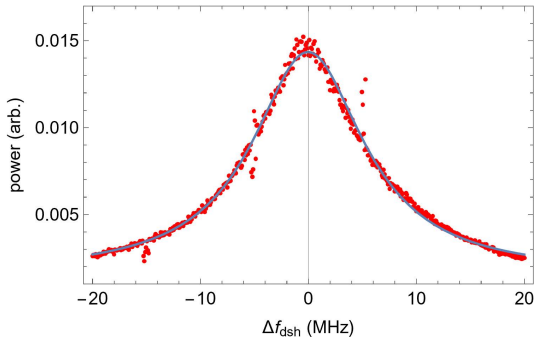

Fig. 5. An example of the delayed self-heterodyne spectrum for the frequency-stabilized (locked) laser and the Lorentzian fit to the data used to determine the laser linewidth. The narrow features that appear near -15, -5, and 5 MHz result from technical noise in the spectrum analyzer and are not caused by the laser light. Here Δf_{dsh} is the frequency deviation from the nominal beatnote of 675 MHz set by the EOM drive frequency.

B. Absorption data

We also observe the water lines near 1389.8 nm using absorption spectroscopy. The optical setup is identical to Fig. 1, but with the rf electronics off so that no sidebands are generated by the EOM and the signal from the balanced photodiode is recorded directly. The frequency of the laser is again scanned by ramping the temperature, resulting in the absorption spectrum shown in Fig. 6. The largest absorption line in this range, near -10.5 GHz, is used to stabilize the laser frequency via the EOM first-order sideband as described above, and corresponds to the absorption line labeled as 7194.805279 cm^{-1} in the Hitran database [29]. The weaker absorption line near 12.4 GHz, corresponding to 7195.566533 cm^{-1} in the Hitran database, causes the small, secondary lineshape that appears in Fig. 2 as the (opposite) first-order sideband scans across this resonance.

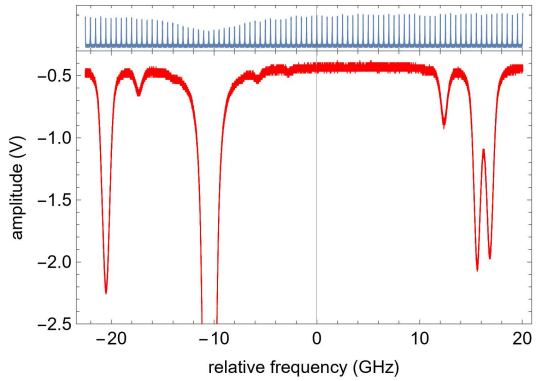

Fig. 6. The measured water vapor absorption as the laser frequency is scanned around 1389.8 nm. In this plot, zero relative frequency corresponds to the DFB laser frequency when the EOM first-order sideband is locked to the water absorption line near -10.5 GHz. The small plot at the top shows transmission peaks through a Fabry-Pérot cavity with a free-spectral range of 500.7 MHz, which is used to set the frequency scale.

Funding. U.S. National Science Foundation (1752685).

Acknowledgment. S.O. thanks Tongyao (Cornelia) Wang for early contributions to the water vapor spectroscopy experimental setup.

OPTICS CONTINUUM

Disclosures. The authors declare no conflicts of interest. Specific product citations are for the purpose of technical clarification only, and are not an endorsement by the authors, the National Science Foundation, or Denison University.

Data availability. Data underlying the results presented in this paper are not publicly available at this time but may be obtained from the authors upon reasonable request.

References

1. E. Grumbling and M. Horowitz, *Quantum Computing: Progress and Prospects* (The National Academies Press, 2019).
2. J. Eschner, G. Morigi, F. Schmidt-Kaler, *et al.*, "Laser cooling of trapped ions," J. Opt. Soc. Am. B **20**(5), 1003–1015 (2003).
3. H. J. Metcalf and P. van der Straten, "Laser cooling and trapping of atoms," J. Opt. Soc. Am. B **20**(5), 887–908 (2003).
4. M. R. Tarbutt, "Laser cooling of molecules," Contemp. Phys. **59**(4), 356–376 (2018).
5. A. D. Ludlow, M. M. Boyd, J. Ye, *et al.*, "Optical atomic clocks," Rev. Mod. Phys. **87**(2), 637–701 (2015).
6. X. Zhang and J. Ye, "Precision measurement and frequency metrology with ultracold atoms," Natl. Sci. Rev. **3**(2), 189–200 (2016).
7. C. L. Degen, F. Reinhard, and P. Cappellaro, "Quantum sensing," Rev. Mod. Phys. **89**(3), 035002 (2017).
8. J. Ye and P. Zoller, "Quantum sensing with atomic, molecular, and optical platforms for fundamental physics," Phys. Rev. Lett. **132**(19), 190001 (2024).
9. C. D. Bruzewicz, J. Chiaverini, R. McConnell, *et al.*, "Trapped-ion quantum computing: progress and challenges," Appl. Phys. Rev. **6**(2), 021314 (2019).
10. C. Hempel, *Trapped-Ion Quantum Computers* (Springer Nature, 2026), pp. 15–24.
11. E. W. Streed, T. J. Weinhold, and D. Kielpinski, "Frequency stabilization of an ultraviolet laser to ions in a discharge," Appl. Phys. Lett. **93**(7), 071103 (2008).
12. M. W. Lee, M. C. Jarratt, C. Marciniak, *et al.*, "Frequency stabilization of a 369 nm diode laser by nonlinear spectroscopy of ytterbium ions in a discharge," Opt. Express **22**(6), 7210–7221 (2014).
13. D. R. Leibrandt, M. J. Thorpe, M. Notcutt, *et al.*, "Spherical reference cavities for frequency stabilization of lasers in non-laboratory environments," Opt. Express **19**(4), 3471–3482 (2011).
14. T. Chen, J. Kim, M. Kuzyk, *et al.*, "Stable turnkey laser system for a Yb/Ba trapped-ion quantum computer," IEEE Trans. Quantum Eng. **3**, 1–8 (2022).
15. J. Valencia, G. Iskander, N. V. Nardelli, *et al.*, "Cryogenic sapphire optical reference cavity with crystalline coatings at 1×10^{-16} fractional frequency instability," Rev. Sci. Instrum. **95**(10), 103002 (2024).
16. B. Kraus, S. Herbers, C. Nauk, *et al.*, "Ultra-stable transportable ultraviolet clock laser using cancellation between photo-thermal and photo-birefringence noise," Opt. Lett. **50**(2), 658–661 (2025).
17. G. P. Barwood, P. Gill, G. Huang, *et al.*, "Automatic laser control for a $^{88}Sr^{+}$ optical frequency standard," Meas. Sci. Technol. **23**(5), 055201 (2012).
18. S. Hannig, L. Pelzer, N. Scharnhorst, *et al.*, "Towards a transportable aluminium ion quantum logic optical clock," Rev. Sci. Inst. **90**(5), 053204 (2019).
19. M. Ghadimi, E. M. Bridge, J. Scarabel, *et al.*, "Multichannel optomechanical switch and locking system for wavemeters," Appl. Opt. **59**(17), 5136–5141 (2020).
20. S. Olmschenk, K. C. Younge, D. L. Moehring, *et al.*, "Manipulation and detection of a trapped Yb^{+} hyperfine qubit," Phys. Rev. A **76**(5), 052314 (2007).
21. T. Dutta, D. D. Munshi, and M. Mukherjee, "Absolute Te_2 reference for barium ion at 455.4nm," J. Opt. Soc. Am. B **33**(6), 1177–1181 (2016).
22. T. Xie, N. Jin, Y. Wang, *et al.*, "Frequency stabilization of a 650nm laser to an I_2 spectrum for trapped $^{138}Ba^{+}$ ions," J. Opt. Soc. Am. B **36**(2), 243–247 (2019).
23. H. Wu, P. Lu, Y. Liu, *et al.*, "Frequency stabilization of a 739nm laser to an I_2 spectrum for trapped ytterbium ions," J. Opt. Soc. Am. B **39**(5), 1457–1461 (2022).
24. Y. Wu, B. Sun, and X. Li, "Semiconductor laser active frequency stabilization technologies: a review," J. Korean Phys. Soc. **79**(9), 795–809 (2021).
25. M. Mäusezahl, F. Munkes, and R. Löw, "Tutorial on laser locking techniques and the manufacturing of vapor cells for spectroscopy," New J. Phys. **26**(10), 105002 (2024).
26. M. T. Hummon, S. Kang, D. G. Bopp, *et al.*, "Photonic chip for laser stabilization to an atomic vapor with 10^{-11} instability," Optica **5**(4), 443–449 (2018).
27. J. Ding, G. Yu, D. You, *et al.*, "Compact and high reliable frequency-stabilized laser system at 589 nm based on the distributed-feedback laser diodes," Appl. Phys. B **127**(9), 130 (2021).
28. T. Dennis, E. A. Curtis, C. W. Oates, *et al.*, "Wavelength references for 1300-nm wavelength-division multiplexing," J. Lightwave Technol. **20**(5), 776–782 (2002).
29. I. Gordon, L. Rothman, R. Hargreaves, *et al.*, "The HITRAN2020 molecular spectroscopic database," J. Quant. Spectrosc. Radiat. Transfer **277**, 107949 (2022).
30. O. Grohe, H. Gottschling, H. Jennewein, *et al.*, "Frequency stabilization of a semiconductor laser using water-vapor absorption lines," Opt. Eng. **40**(4), 529–532 (2001).

OPTICS CONTINUUM

31. H. Tsuchida, M. Ohtsu, and T. Tako, "Frequency stabilization of AlGaAs semiconductor laser to the absorption line of water vapor," Jpn. J. Appl. Phys. **21**(1A), L1 (1982).
32. V. Pevtschin and S. Ezekiel, "Investigation of absolute stability of water-vapor-stabilized semiconductor laser," Opt. Lett. **12**(3), 172–174 (1987).
33. A. Dinovitser, L. J. Gunn, and D. Abbott, "Towards quantitative atmospheric water vapor profiling with differential absorption lidar," Opt. Express **23**(17), 22907–22921 (2015).
34. G. Galzerano and P. Laporta, "Frequency-stabilized seed laser system for dial applications around 0.94μm," Optics and Lasers in Engineering **44**(7), 677–686 (2006).
35. G. J. Koch, A. L. Cook, C. M. Fitzgerald, *et al.*, "Frequency stabilization of a diode laser to absorption lines of water vapor in the 944-nm wavelength region," Opt. Eng. **40**(4), 525–528 (2001).
36. R. Matthey, S. Schilt, D. Werner, *et al.*, "Diode laser frequency stabilisation for water-vapour differential absorption sensing," Appl. Phys. B **85**(2-3), 477–485 (2006).
37. A. Fix, G. Ehret, J. Löhring, *et al.*, "Water vapor differential absorption lidar measurements using a diode-pumped all-solid-state laser at 935 nm," Appl. Phys. B **102**(4), 905–915 (2011).
38. Z. Wang, J. Chang, H. Yu, *et al.*, "Multi-component and multi-point trace gas sensing in wavelength modulation spectroscopy based on wavelength stabilization," Photonic Sens. **9**(4), 376–387 (2019).
39. J. L. Nowak, P. Magryta, T. Stacewicz, *et al.*, "Fast optoelectronic sensor of water concentration," Optica Appl. **46**, 607–618 (2016).
40. W. Gurlit, R. Zimmermann, C. Giesemann, *et al.*, "Lightweight diode laser spectrometer CHILD (Compact High-altitude In-situ Laser Diode) for balloonborne measurements of water vapor and methane," Appl. Opt. **44**(1), 91 (2005).
41. C. M. Fitzgerald, "Wavelength modulation spectroscopy of water vapor and line center stabilization at 1.462 μm for lidar applications," Master of Science (MS) thesis (Old Dominion University, 2000), https://digitalcommons.odu.edu/ece_etds/339.
42. D. Werner, S. Schilt, L. Thévenaz, *et al.*, "Laser frequency stabilization using direct and offset locking techniques," in *DGaO-Proceedings*, vol. 105, (Deutschen Gesellschaft für angewandte Optik (DGaO), 2004), p. P51.
43. G. Gagliardi, G. Rusciano, and L. Gianfrani, "Sub-doppler spectroscopy of $H_2{}^{18}O$ at 1.4 μm," Appl. Phys. B **70**(6), 883–888 (2000).
44. G. Galzerano, E. Fasci, A. Castrillo, *et al.*, "Absolute frequency stabilization of an extended-cavity diode laser against Doppler-free $H_2{}^{17}O$ absorption lines at 1.384 μm," Opt. Lett. **34**(20), 3107–3109 (2009).
45. H. Dinesan, E. Fasci, A. Castrillo, *et al.*, "Absolute frequency stabilization of an extended-cavity diode laser by means of noise-immune cavity-enhanced optical heterodyne molecular spectroscopy," Opt. Lett. **39**(7), 2198–2201 (2014).
46. H. Dinesan, E. Fasci, A. D'Addio, *et al.*, "Characterization of the frequency stability of an optical frequency standard at 1.39 μm based upon noise-immune cavity-enhanced optical heterodyne molecular spectroscopy," Opt. Express **23**(2), 1757–1766 (2015).
47. M. Melosso, M. L. Diouf, L. Bizzocchi, *et al.*, "Hyperfine-resolved near-infrared spectra of $H_2{}^{17}O$," J. Phys. Chem. A **125**(36), 7884–7890 (2021).
48. S. Olmschenk, "Doubly ionized lanthanum as a qubit candidate for quantum networks," Phys. Rev. A **105**(4), 042617 (2022).
49. M. A. Tran, D. Huang, and J. E. Bowers, "Tutorial on narrow linewidth tunable semiconductor lasers using Si/III-V heterogeneous integration," APL Photonics **4**(11), 111101 (2019).
50. P. C. D. Hobbs, *Building Electro-Optical Systems: Making It All Work* (John Wiley & Sons, Inc., 2022), chap. Front Ends, pp. 652–653, 3rd ed.
51. S. Olmschenk, P. R. Banner, J. Hankes, *et al.*, "Optogalvanic spectroscopy of the hyperfine structure of the $5p^6 5d^2 D_{3/2,5/2}$ and $5p^6 4f^2 F^o_{5/2,7/2}$ levels of La III," Phys. Rev. A **96**(3), 032502 (2017).
52. W. Riley and D. A. Howe, "Handbook of frequency stability analysis," Tech. Rep. 1065, National Institute of Standards and Technology, Gaithersburg, MD (2008). Special Publication (NIST SP).
53. B. B. Blinov, R. N. Kohn, M. J. Madsen, *et al.*, "Broadband laser cooling of trapped atoms with ultrafast pulses," J. Opt. Soc. Am. B **23**(6), 1170–1173 (2006).
54. T. Lindvall, T. Fordell, I. Tittonen, *et al.*, "Unpolarized, incoherent repumping light for prevention of dark states in a trapped and laser-cooled single ion," Phys. Rev. A **87**(1), 013439 (2013).
55. N. C. Wong and J. L. Hall, "Servo control of amplitude modulation in frequency-modulation spectroscopy: demonstration of shot-noise-limited detection," J. Opt. Soc. Am. B **2**(9), 1527–1533 (1985).
56. W. Zhang, M. J. Martin, C. Benko, *et al.*, "Reduction of residual amplitude modulation to 1×10^{-6} for frequency modulation and laser stabilization," Opt. Lett. **39**(7), 1980–1983 (2014).
57. M. Descampeaux, G. Feugnet, and F. Bretenaker, "New method for residual amplitude modulation control in fibered optical experiments," Opt. Express **29**(22), 36211–36225 (2021).
58. A. Kramida, Yu. Ralchenko, and J. Reader, and NIST ASD Team, "NIST Atomic Spectra Database," National Institute of Standards and Technology, ver. 5.12 (2024), https://physics.nist.gov/asd.
59. R. A. Carollo, D. A. Lane, E. K. Kleiner, *et al.*, "Third-harmonic-generation of a diode laser for quantum control of beryllium ions," Opt. Express **25**(7), 7220–7229 (2017).
60. R. Cazan, C. Geppert, W. Nörtershäuser, *et al.*, "Towards sympathetic cooling of trapped ions with laser-cooled Mg^+ ions for mass spectrometry and laser spectroscopy," Hyperfine Interact. **196**(1-3), 177–189 (2010).

OPTICS CONTINUUM

61. S. Ranta, M. Tavast, T. Leinonen, *et al.*, "Narrow linewidth 1118/559 nm VECSEL based on strain compensated GaInAs/GaAs quantum-wells for laser cooling of Mg-ions," Opt. Mater. Express **2**(8), 1011–1019 (2012).
62. P. Müller, A. Tretiakov, A. Younes, *et al.*, "Hyperfine spectroscopy of optical-cycling transitions in singly ionized thulium," Sci. Rep. **16**(1), 10655 (2026).
63. S. Mulholland, H. A. Klein, G. P. Barwood, *et al.*, "Compact laser system for a laser-cooled ytterbium ion microwave frequency standard," Rev. Sci. Instrum. **90**(3), 033105 (2019).
64. S. M. Spuler, M. Hayman, and T. M. Weckwerth, *Water Vapor Differential Absorption Lidar* (Springer International Publishing, 2021) pp. 741–757.